

Study of $\text{HgBa}_2\text{CuO}_{4+\delta}$ by Angle-Resolved Photoemission Spectroscopy

W.S. Lee,¹ T. Yoshida,¹ W. Meevasana,¹ K.M. Shen,¹ D.H. Lu,¹ W.L. Yang,² X.J. Zhou,² X. Zhao,¹ G. Yu,¹ Y. Cho,¹ M. Greven,¹ Z. Hussain,² and Z.-X. Shen¹

¹*Department of Physics, Applied Physics, and Stanford Synchrotron Radiation Laboratory, Stanford University, Stanford, CA 94305*

²*Advanced Light Source, Lawrence Berkeley National Lab, Berkeley, CA 94720*

(Dated: June 27, 2018)

We present the first angle-resolved photoemission measurement on the single-layer Hg-based cuprate, $\text{HgBa}_2\text{CuO}_{4+\delta}$ (Hg1201). A quasi-particle peak in the spectrum and a kink in the band dispersion around the diagonal of the Brillouin zone are observed, whereas no structure is detected near the Brillouin zone boundary. To search for a material-dependent trend among hole-doped cuprates, including Hg1201, we use a tight-binding model to fit their Fermi surfaces. We find a positive correlation between the $T_{c,\text{max}}$ and t'/t , consistent with theoretical predictions.

PACS numbers: Valid PACS appear here

Empirically, it is known that the maximum transition temperature, $T_{c,\text{max}}$, varies strongly among different high- T_c superconducting compounds¹. For example, the single-layer compounds, $\text{Bi}_2\text{Sr}_2\text{CuO}_{6+\delta}$ (Bi2201) and $\text{La}_{2-x}\text{Sr}_x\text{CuO}_4$ (LSCO), have a $T_{c,\text{max}}$ of ~ 40 K, while $\text{HgBa}_2\text{CuO}_{4+\delta}$ (Hg1201) and $\text{Tl}_2\text{Ba}_2\text{CuO}_{6+\delta}$ (Tl2201) have a $T_{c,\text{max}}$ of 98 K and 93 K, respectively. This material dependence has been related to disorder and crystal structure^{1,2}. The latter determines the hybridizations of the Cu orbitals with those of other elements, resulting in different values of hopping integrals in the effective single-band tight-binding Hamiltonian for distinct compounds^{3,4}. However, experimental studies which directly address this material dependence of the band structure have not been extended to compounds with the highest $T_{c,\text{max}}$ ^{5,6}, due to the lack of sufficiently large high-quality single crystals for the materials with higher $T_{c,\text{max}}$. Fortunately, through significantly improved crystal growth techniques, sizable single crystals of Hg1201 have recently become available⁷. Because Hg1201 has the highest $T_{c,\text{max}}$ among all single-layer cuprates⁸ and possesses a relatively simple tetragonal crystal structure², it is an ideal system to complement this material dependence issue. Until now, spectroscopy studies on this system have been limited to angle-integrated photoemission⁹ or to a small momentum transfer region, such as Raman spectroscopy¹⁰; the momentum space properties of the electronic states, such as the band dispersions and the Fermi surface (FS), are not yet available.

In this article, we report the first angle-resolved photoemission spectroscopy (ARPES) results on nearly optimally-doped Hg1201 crystals ($T_c=96$ K). With the unique ability of ARPES to resolve states in the momentum-energy space¹¹, we observed a single sheet of the Fermi surface and a kink in the dispersion along the diagonal of the zone (nodal direction). Our analysis provides an opportunity to examine two universal properties of the cuprates: (1) the positive correlation between the effective single-band parameter, t'/t , and $T_{c,\text{max}}$; (2) the existence of an energy scale related to the electron-boson

coupling.

Single crystals of Hg1201 were grown at Stanford University using a significantly improved melt-growth method⁷. Small pieces, with a typical size of $0.7 \times 0.7 \times 0.5$ mm³, were selected for ARPES measurements. The crystals were polished and cleaned using a bromine solution (5% Br + 95% ethanol) until the surface was shiny. The crystals were then annealed at 300°C under oxygen flow; finally, nearly optimally-doped crystals with a T_c of 96 K and a transition width of less than 3 K were obtained, as shown in Fig. 1(b). The bromine treatment of the surface is applied again immediately before mounting the samples to reduce the surface contact resistance. A typical four-fold symmetric Laue pattern of the [001] surface is shown in Fig. 1(c).

The ARPES experiments were performed at beamline 5-4 of the Stanford Synchrotron Radiation Laboratory (SSRL) and beamline 10.0.1 of the Advanced Light Source (ALS) with SCIENTA SES200 and R4000 electron analyzers, respectively. The energy resolution was set at 20-25 meV. We used 19 eV photons at the SSRL and 55 eV photons at the ALS to excite the electrons. The samples were oriented *ex situ* using Laue diffraction, then cleaved *in situ* and measured at a temperature of approximately 15K under ultra high vacuum at a pressure lower than 4×10^{-11} Torr. Perhaps due to the absence of a natural cleaving plane in the crystal structure (Fig. 1(a)), the cleaved surface of Hg1201 is generally rough, and the signal is weaker compared to the other most studied cuprates, such as Bi2212 and LSCO. However, a LEED pattern can still be observed as shown in Fig. 1(d), suggesting that a portion of the surface layer still preserves good periodicity after cleaving.

The grey scale intensity plot of the ARPES spectrum along the nodal direction is illustrated in Fig. 2(a), where a band dispersion can be observed. Corresponding energy distribution curves (EDCs) are plotted in Fig. 2(c). A quasi-particle-like peak can be observed near the Fermi crossing point, k_F (the thick curve in Fig. 2(c)) and rapidly fades into a step-like background. To better visualize the band dispersion, the EDCs were first normal-

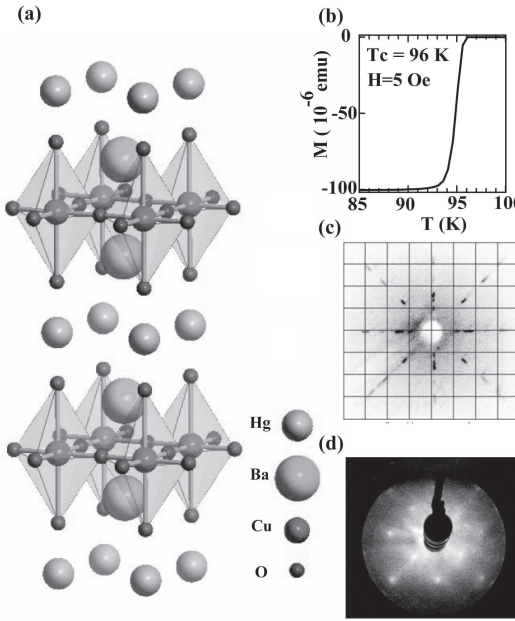


FIG. 1: (a) Crystal structure of Hg1201; (b) Zero field cooled magnetic moment curve of Hg1201; (c) Laue pattern of Hg1201 representing the [001] surface, the a-b plane; (d) LEED pattern of the cleaved surface.

ized between 500 meV and 520 meV below the Fermi energy; we then subtracted the normalized background (Fig. 2(d)). The background-removed spectra are shown in Fig. 2(b) and the corresponding EDCs are displayed in Fig. 2(e). Moving away from nodal region toward the antinodal region along Fermi surface, this quasi-particle peak diminishes, as illustrated in Fig. 2(f). Near the antinodal region, the EDCs primarily consist of a step-like background with no sharp quasi-particle-like peak in either the raw or the background subtracted EDCs.

The appearance of this step-like background throughout the zone is likely an angle-integrated spectrum due to the roughness of the cleaved surface. We note that this background is gapped, with a spectral weight suppression between -30 meV to E_F . This is consistent with the angle-integrated photoemission spectrum reported on the same material⁹, suggesting a maximum superconducting gap size of approximately 30 meV or larger.

The absence of a quasi-particle-like peak around the antinodal region is, however, puzzling. Since the T_c (96 K) of our samples is comparable to the optimally-doped double-layer system Bi2212, a sharp peak with high intensity in the antinodal region as in Bi2212 is expected¹². This antinodal peak, if it exists, should not be washed out by the angle-integrated background, especially when a nodal quasi-particle peak is present. Therefore, we suspect that the absence of the antinodal peaks is either a result of broken crystal symmetry at the surface, or an intrinsic feature of the nearly optimally-doped Hg1201. For the latter, we note that it might be similar to the case of LSCO in which there exists a dichotomy electronic states

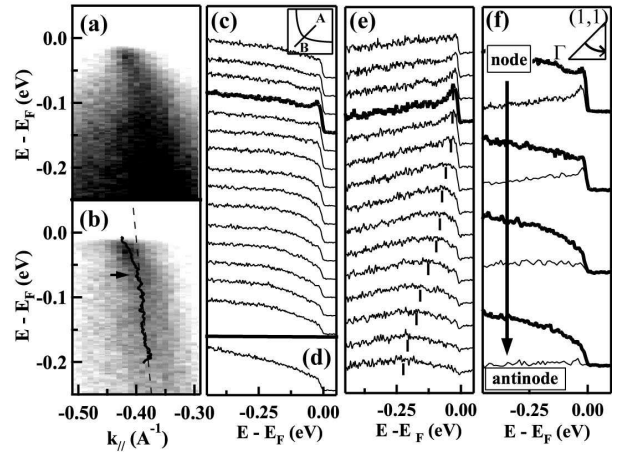


FIG. 2: (a) Grey scale intensity plot of the raw ARPES spectrum along $(0,0)$ - $(1,1)$ direction; (b) Spectrum with background [illustrated in (d)] subtracted from (a). The MDC-derived band dispersion is illustrated by the solid curve; the kink is indicated by the black arrow. (c),(e) EDC stack plots of (a) and (b), respectively. Bars in (e) indicate the band dispersion in EDCs. (d) The EDC of the background selected at a position of $k \gg k_F$. (f) EDCs along the Fermi surface as illustrated in the inset. The thicker curves represent the raw data; the thinner curves illustrate the background removed data.

in the nodal region and antinodal region¹⁶; the antinodal peak may emerge only at higher doping levels. A doping dependence study of Hg1201 will be necessary to clarify this issue.

In Fig. 3, we show the FS of Hg1201, which was taken using 55 eV photons at the ALS. As expected, a single sheet of FS is observed. With our experimental setup, the spectral weight in the second and fourth quadrants is strongly suppressed due to the matrix element effect. The Fermi crossing points are determined by fitting the peak positions of momentum distribution curves (MDCs) near the Fermi energy, as shown in the inset of Fig. 3. The FS, illustrated by the solid symbols in Fig. 3, is extracted up to the antinodal region where the MDC peaks disappear. We note that by collecting data in symmetric quadrants on the same sample, the symmetry requirement of the FS enables us to determine the position of the Fermi crossing points more accurately. In particular, averaging three data sets taken on different samples at the ALS and SSRL, we determine the Fermi crossing point along the nodal direction, (k_n, k_n) , to be $k_n = 0.374 \pm 0.006$, in units of π/a .

Compared to other nearly optimally-doped cuprates, k_n of Hg1201 is relatively small, close to that of materials with a higher $T_{c,\max}$, as shown in Table I. The variation in k_n among nearly optimally-doped compounds, which presumably possess a similar doping level, suggests a difference of band structures for these systems. Setting aside strong correlations, such as the electron-electron interaction and renormalization effects from bosonic chan-

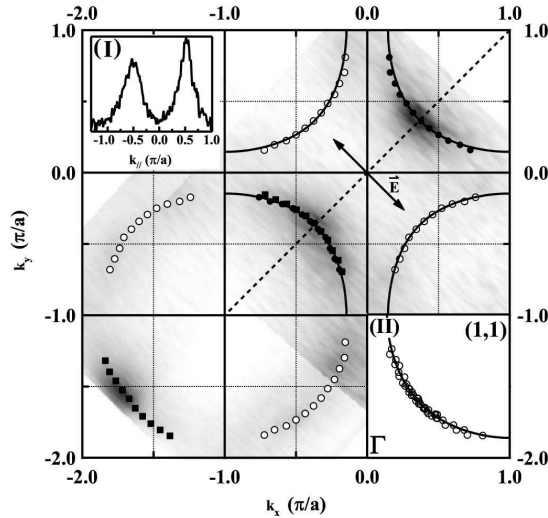


FIG. 3: Fermi surface of the Hg1201 generated by integrating the spectrum ± 10 meV with respect to E_F . The solid symbols represent the Fermi crossing points, k_F , determined by the peak positions of the MDC near E_F . The open symbols are symmetrized from the solid symbols. The solid curve is the tight-binding FS as described in the text. The inset (I) shows the MDC around E_F along the dashed line. The inset (II) illustrates the Fermi crossing points collected from three sets of data which were taken at the SSRL and ALS. The fitted tight binding FS is also shown.

nel (e.g. phonons and spin excitations), we use a tight-binding model to describe the Fermi surface. Including up to the second nearest-neighbor hopping term, the FS of the tight-binding model is given by

$$0 = \frac{\mu}{t} - 2(\cos k_x + \cos k_y) + 4\frac{t'}{t} \cos k_x \cos k_y, \quad (1)$$

where t and t' represent the nearest-neighbor and the second nearest-neighbor hopping integral on Cu-O plane, respectively. Based on Eq. 1, we then perform a least-square fit for the Fermi crossing points of various cuprates listed in Table I. The Fermi crossing points of each compound are collected from at least two sets of data, which are either published results (e.g. Tl2201 data) or the data from our own group. As an example, we show the Fermi crossing points of the Hg1201 system in the inset (II) of Fig. 3, which contains three data sets collected at the SSRL and ALS; the FS obtained from the tight-binding fit is also plotted. Finally, the ratio t'/t obtained from our analysis is summarized in Table I.

To search for a material dependent trend, we plot t'/t versus the $T_{c,\max}$ of the corresponding compound in Fig. 4; a positive correlation between the t'/t and the $T_{c,\max}$ is revealed. In the absence of FS data for optimally doped Tl2201, the values of t'/t obtained from the over-doped Tl2201 ($T_c = 20\sim 30$ K)^{14,15} was used to represent those of the corresponding optimally doped compounds. We note that the accuracy of t'/t for Tl2201 compound

TABLE I: node position k_n , T_c , $T_{c,\max}$, and t'/t obtained from the tight-binding analysis for various cuprates. Relevant references were also included.

	k_n ^a	T_c (K)	$T_{c,\max}$	t'/t^b	t'/t^c	reference
Hg1201	0.374	96	98	0.408	0.249	¹³
Bi2223	0.367	110	110	0.429	0.277	¹
Bi2212	0.381	96	96	0.407	0.247	¹
Tl2201	0.357	$20\sim 30$	93	0.433	0.251	^{14,15}
LSCO	0.400	40	40	0.293	0.162	^{16,17}
Bi2201	0.397	35	35	0.371	0.204	¹

^aFor Tl2201, k_n was obtained by digitizing the FS shown in the Ref.¹⁴; others values were obtained directly from our group's data.

^bObtained by fitting FS to the $t - t'$ model.

^cObtained by fitting FS to the $t - t' - t''$ model with the constrain $t'' = 0.5t'$.

should be verified, once data for optimally-doped crystals are available. We also tried to extend our tight-binding model to include the third nearest-neighbor hopping term, $-2\frac{t''}{t}(\cos 2k_x + \cos 2k_y)$. However, we find that the fitting process does not converge very well; there exist many possible sets of t'/t , t''/t , and μ/t yielding good fits to the data. This is because the current FS data are not accurate enough to uniquely determine the fitting parameters. To avoid this difficulty, we set t'' to its leading-order value, $t'/2^3$, such that the fitting process is robust. The fitted t'/t is summarized in Table I and plotted in the inset (I) of Fig. 4; similarly, the positive correlation between $T_{c,\max}$ and t'/t is observed.

This correlation is consistent with theoretical calculations^{3,4}, although the correlation revealed from our analysis is less monotonic than that from the theory (inset (II) of Fig. 4). This is probably due to the limited accuracy of our analysis and the strong correlation effects, which are not captured by our analysis or band structure calculations. Nevertheless, the qualitative agreement between our analysis and the theories lends support to the theoretical proposal^{3,4} that the crystal-structure along the c -axis, especially the apical oxygen atom, can manifest itself in the effective single-band structure of the $a - b$ plane. Furthermore, it has also been shown by the mean-field calculations for the $t - J$ model that a higher t'/t ratio can enhance the stability of the superconducting pairs^{18,19}. This is also consistent with the positive correlation between $T_{c,\max}$ and t'/t . We remark that the correlation observed here is probably only one factor of the material dependence of $T_{c,\max}$, as there are other factors that could also affect $T_{c,\max}$. For example, although LSCO possesses a lower values of $T_{c,\max}$ and t'/t , the competing orders in this system, such as stripes¹⁶, could also suppress the $T_{c,\max}$.

Our data also confirm another universal property of the cuprates: the existence of an energy scale which is related to the electron-boson coupling. In Fig. 2(b), we superpose the MDC-derived band dispersion on the grey scale intensity plot of the spectrum. A kink in the dispersion between 60 meV to 80 meV is observed. This

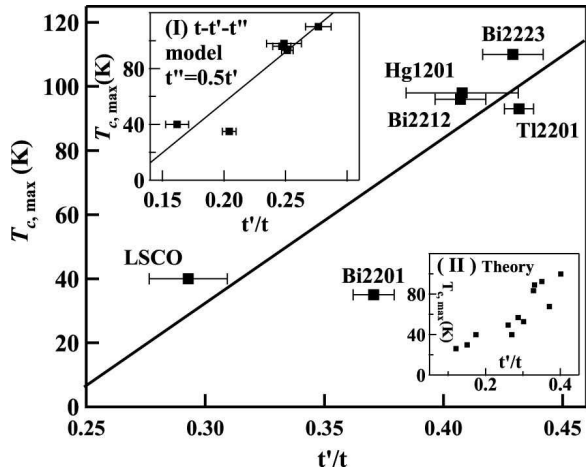


FIG. 4: Positive correlation between $T_{c,\max}$ and t'/t . Inset (I) is the results obtained from $t - t' - t''$ model. Error bars are the 99% confidence interval of the fitted t'/t . Inset (II) is reproduced from Ref.³. The lines in the figures are guides-to-the eye, indicating the positive correlation between $T_{c,\max}$ and t'/t .

feature has also been observed in other cuprates²⁰, suggesting that it is a universal feature in cuprates. This dispersion kink has recently attracted a lot of attention in the high T_c community and has been thought to be a signature of electrons coupled to some bosons, whose origins are still strongly debated^{20,21}. Possible candidates in

the case of Hg1201 system include the following modes: (1) the A_{1g} 590 cm^{-1} phonon mode observed in the Raman spectrum, which shows a superconductivity-induced anomaly¹⁰; (2) the bond stretching phonon, which shows an unusual softening at a similar energy²²; (3) a mode of magnetic origin²³. More detailed studies are needed to identify the origin of the bosonic mode(s) in Hg1201.

In conclusion, we report the first ARPES results of the nearly optimally-doped Hg1201 crystals. A tight-binding analysis on the FS of various optimally-doped cuprates is also illustrated, which suggests a positive correlation between t'/t and the $T_{c,\max}$. However, a more complete analysis, which takes the strong correlation effects into account, is necessary to gain deeper insight into the material dependence issue. Regarding the universality of the electron-boson coupling in cuprates, further studies covering a broader range of materials and doping levels are required for a comprehensive understanding.

W.S. Lee thanks S. Maekawa, T. Devereaux, F. Baumberger, and O.K. Andersen for useful discussions. SSRL is operated by the DOE Office of Basic Energy Science, Division of Chemical Science and Material Science under contract DE-AC03-765F00515. The ARPES measurements at Stanford were also supported by NSF DMR-0304981, ONR Grant No. N00014-0501-0127. The crystal growth was supported by DOE Contracts No. DE-FG03-99ER45773 and DE-AC03-76F00515, and by NFS DMR 9985067.

¹ H. Eisaki, N. Kaneko, D. L. Feng, A. Damascelli, P. K. Mang, K. M. Shen, Z.-X. Shen, and M. Greven, Phys. Rev. B **69**, 064512 (2004), and references therein.

² J. D. Jorgensen *et al.*, in *Recent Developments in High Temperature Superconductivity*, Edited by J. Klamut, *et. al.*, (Springer, New York, 1996), p. 4.

³ E. Pavarini, I. Dasgupta, T. Saha-Dasgupta, O. Jepsen, and O. K. Andersen, Phys. Rev. Lett. **87**, 047003 (2001).

⁴ R. Raimondi, J. H. Jefferson, and L. F. Feiner, Phys. Rev. B **53**, 8774 (1996).

⁵ Y.-J. Kim, J. P. Hill, G. D. Gu, F. C. Chou, S. Wakimoto, R. J. Birgeneau, Seiki Komiya, Yoichi Ando, N. Motoyama, K. M. Kojima, S. Uchida, D. Casa, and T. Gog, cond-mat/0407179.

⁶ K. Tanaka, T. Yoshida, A. Fujimori, D. H. Lu, Z.-X. Shen, X.-J. Zhou, H. Eisaki, Z. Hussain, S. Uchida, Y. Aiura, K. Ono, T. Sugaya, T. Mizuno, and I. Terasaki, Phys. Rev. B **70**, 092503 (2004).

⁷ X. Zhao, G. Yu, Y. Cho, N. Barisic, P. Bourges, N. Kaneko, Y. Li, L. Lu, E. M. Motoyama, O. P. Vajk, and M. Greven, cond-mat/0604103.

⁸ S. N. Putilin, E. V. Antipov, O. Chmaissem, and M. Marezio, Nature **362**, 226 (1993).

⁹ H. Uchiyama, W.-Z. Hu, A. Yamamoto, S. Tajima, K. Saiki, and A. Koma, Phys. Rev. B **62**, 615 (2000).

¹⁰ e.g. M. C. Krantz, C. Thomsen, H. J. Mattausch, and M. Cardona, Phys. Rev. B **50**, 1165 (1994).

¹¹ A. Damascelli, Z. Hussain, and Z.-X. Shen, Rev. Mod. Phys. **75**, 473 (2003).

¹² D. L. Feng, D. H. Lu, K. M. Shen, C. Kim, H. Eisaki, A. Damascelli, R. Yoshizaki, J.-i. Shimoyama, K. Kishio, G. D. Gu, S. Oh, A. Andrus, J. O'Donnell, J. N. Eckstein, Z.-X. Shen, Science **289**, 277 (2000).

¹³ A. Yamamoto, W.-Z. Hu, and S. Tajima, Phys. Rev. B **63**, 024504 (2000).

¹⁴ M. Plate, J. D. F. Mottershead, I. S. Elfimov, D. C. Peets, Ruixing Liang, D. A. Bonn, W. N. Hardy, S. Chiuzbaian, M. Falub, M. Shi, L. Patthey, and A. Damascelli, Phys. Rev. Lett. **95**, 077001 (2005).

¹⁵ N. E. Hussey, M. Abdel-Jawad, A. Carrington, A. P. Mackenzie and L. Balicas, Nature **425**, 814 (2003).

¹⁶ X. J. Zhou, T. Yoshida, S. A. Kellar, P. V. Bogdanov, E. D. Lu, A. Lanzara, M. Nakamura, T. Noda, T. Kakeshita, H. Eisaki, S. Uchida, A. Fujimori, Z. Hussain, and Z.-X. Shen, Phys. Rev. Lett. **86**, 5578 (2001).

¹⁷ A. Ino, C. Kim, M. Nakamura, T. Yoshida, T. Mizokawa, A. Fujimori, Z.-X. Shen, T. Kakeshita, H. Eisaki, and S. Uchida, Phys. Rev. B **65**, 094504 (2002).

¹⁸ C. T. Shih, T. K. Lee, R. Eder, C.-Y. Mou, and Y. C. Chen, Phys. Rev. Lett. **92**, 227002 (2004).

¹⁹ X. J. Chen and H. Q. Lin, Phys. Rev. B **69**, 104518 (2004).

²⁰ A. Lanzara, P. V. Bogdanov, X. J. Zhou, S. A. Kellar, D. L. Feng, E. D. Lu, T. Yoshida, H. Eisaki, A. Fujimori, K. Kishio, J.-i. Shimoyama, T. Noda, S. Uchida, Z. Hussain

and Z.-X. Shen *et al.*, *Nature* **412**, 510 (2001).

²¹ M. Eschrig and M. R. Norman, *Phys. Rev. Lett.* **85**, 3261 (2000); *Phys. Rev. B* **67**, 144503 (2003).

²² H. Uchiyama, A. Q. R. Baron, S. Tsutsui, Y. Tanaka, W.-Z. Hu, A. Yamamoto, S. Tajima, and Y. Endoh, *Phys. Rev. Lett.* **92**, 197005 (2004).

²³ D. Munoz, F. Illas, and I. de P. R. Moreira, *Phys. Rev. Lett.* **84**, 1579 (2000).